Pergamon

Int. J. Heat Mass Transfer. Vol. 41, Nos 8–9, pp. 1025–1034, 1998

Printed in Great Britain
0017-9310/98 $19.00+0.00

PII: S0017-9310(97)00205-6

A study of the flow field of a confined and submerged impinging jet

JANICE A. FITZGERALD and SURESH V. GARIMELLA†

Department of Mechanical Engineering, University of Wisconsin—Milwaukee, P.O. Box 784, Milwaukee, Wisconsin 53201, U.S.A.

(*Received* 18 *March* 1997 *and in final form* 3 *July* 1997)

Abstract—The flow field of an axisymmetric, confined and submerged turbulent jet impinging normally on a flat plate was studied experimentally using laser–Doppler velocimetry. Single jets of a perfluorinated dielectric liquid (FC-77) issuing from square-edged, geometrically similar nozzles were used in the experiments with the radial outflow confined between parallel plates. The nozzle (length to diameter) aspect ratio was unity, giving rise to a still-developing velocity profile at the nozzle exit. Experiments were conducted with nozzle diameters of 3.18 and 6.35 mm, nozzle-to-target plate spacings of up to four jet diameters, and Reynolds numbers in the range of 8500–23,000. The toroidal recirculation pattern in the outflow region characteristic of confined jets is mapped. Velocities and turbulence levels are presented over a fine measurement grid in the pre-impingement and wall-jet regions. © 1997 Elsevier Science Ltd.

INTRODUCTION

Impinging jets are used in many heat and mass transfer applications because of their effective transport capabilities. Applications include turbine-blade cooling, paper drying and electronics packaging. Trends observed in local heat transfer measurements are closely related to the velocities and turbulence levels of the flow field. Experimental and analytical studies of the flow field in free and submerged jets have provided valuable information regarding their heat transfer characteristics. The presence of a confining top-plate facing the target plate in jet impingement, however, results in a more complicated flow structure, and little information is available in the literature for this configuration. The purpose of the present study is three-fold: to experimentally investigate the characteristics which are unique to confined and submerged impinging jets; to contrast these with the flow fields for free-surface and submerged but unconfined jets; and to interpret the respective heat transfer characteristics in light of the differences in flow fields.

Valuable insight into the heat transfer characteristics of free-surface liquid jets [1–3] and air jets [4–8] (submerged but unconfined) has been gained through the study of their flow fields, but limited work on the effect of confinement in jet impingement has been reported. Investigations of the effect of confinement on heat transfer in air jets [9, 10], planar water jets [11] and axisymmetric liquid jets of a perfluorinated dielectric fluid [12–15] show a resulting reduction in stagnation-region heat transfer. Flow field measurements in the potential core of an air jet show that confinement increases the length of the potential core, decreases turbulence levels in the jet, and reduces the stagnation point heat transfer by up to 10% [16].

In general, the heat transfer to impinging jets can be characterized by the jet Reynolds number, fluid Prandtl number, nozzle geometry (diameter, length and shape), and nozzle-to-target plate spacing. Turbulence levels of the jet play an important role in stagnation heat transfer, with higher levels of turbulence resulting in high stagnation heat transfer. Exit levels of turbulence [1–4, 9] as well as nozzle geometry [10, 13, 16, 17] can affect levels of turbulence at the impingement surface. The mean radial velocity gradient of the jet is reported to be more significant to stagnation heat transfer than turbulence levels in fully developed free jets [2, 3]. The dimensionless velocity gradient is reported to be largely independent of the Reynolds number and the nozzle diameter.

At small nozzle-to-target plate spacings, secondary peaks in the heat transfer distributions have been observed [4, 6, 8, 9, 11–14]. The peaks are more pronounced at small spacings, decreasing in prominence and moving radially away from the jet axis as the spacing increases. Increasing the Reynolds number results in a more pronounced peak, but only slightly affects the location of the peak, moving it away from the jet axis [8, 9, 14]. Confinement is reported to increase the magnitude of the secondary peak in heat transfer distribution for liquid jets [12], but decreases the magnitude of the peaks in air jets [9]. The peaks are generally understood to result from a transition to turbulence in the wall-jet boundary layer, although in the confined jet it is possible that they may also be due to the recirculation pattern found in the outflow region [11].

† Author to whom correspondence should be addressed.

NOMENCLATURE

d	nozzle diameter	u_{rms}	rms of the fluctuating component of local radial velocity
h	local heat transfer coefficient	v	mean component of local axial velocity
H	distance between nozzle plate and target plate	v_c	jet centerline velocity
k	thermal conductivity	V_j	jet mean exit velocity
ℓ	nozzle length (nozzle-plate thickness)	v_{rms}	rms of the fluctuating component of local axial velocity
Nu	Nusselt number (hd/k)	z	coordinate along the jet axis with origin at the target plate.
Pr	Prandtl number (ν/α)	Greek symbols	
r	radius coordinate with origin at the jet axis	α	thermal diffusivity
Re	Reynolds number ($V_j d/\nu$)	ν	kinematic viscosity.
u	mean component of local radial velocity		

EXPERIMENTAL SETUP AND PROCEDURES

The jet impingement facility used in the experiments is a transparent closed-loop system containing a pump, flow meters, and a flow-conditioning plenum at the end of which plates with nozzles of different diameters can be mounted. A jet of FC-77 (a perfluorinated, dielectric liquid with $Pr = 25.3$, $\rho = 1789$ kg m^{-3} and $\nu = 0.86 \times 10^{-6}$ m^2 s^{-1} at 20°C) issues at 20°C from the nozzle into a tank of stagnant fluid at the same temperature and impinges on a target plate. Details of the experimental facility are available in [14]. For the present study, nozzle diameters of 6.35 and 3.18 mm were used with the thickness of the nozzle plate equal to the diameter of the nozzle; a nozzle length-to-diameter aspect ratio (ℓ/d) of one results for both nozzles. The jet velocity profile for this nozzle aspect ratio is neither fully-developed nor uniform, but is still-developing [13]. Nozzle-to-target plate spacings (H/d) of 2, 3 and 4 were studied for each nozzle. The measurements were obtained at three Reynolds numbers ($V_j d/\nu$) of 8500, 13,000 and 23,000. The confinement region bounded by the nozzle and target plates, which is the domain of focus for this study, as well as the measurement locations, are illustrated in Fig. 1.

The velocity and turbulence measurements were obtained with a TSI laser–Doppler velocimeter using a Coherent 2 Watt Argon-ion laser. The 514.5 nm (green) line of the laser was used for both velocity components: the components were measured independently. The focal length of the transmitting lens was 350 mm and the beam spacing was 50 mm. The system is set up in back-scatter mode, with the receiving optics mounted in the same probe as the transmitting optics, and carried by fiber-optic cable to the receiving system where the photomultiplier tubes are located. After the light is converted to an electrical signal and filtered, a TSI model 550 signal processor converts the data from analog to digital which is then fed to a personal computer for analysis. Frequency shifting was used to accurately determine the negative velocities in the flow. Seed particles of corn starch (~ 5 μm diameter) were added to the fluid to provide acceptable data rates. Seven thousand data points were taken at each position to determine the local mean velocity and turbulence level. The averaging was performed over 1000 to 15,000 data points, and the results were found to be independent of sample size for sizes over 5000 data points. The sampling rate varied from approximately 800 to 3000 Hz. A computer-driven, motorized precision traversing system was used to position the measurement volume in the flow field. The traversal resolution in the three directions was ± 0.005 mm, with a placement precision of 0.12 mm m^{-1}.

Before each test, finely-spaced velocities were obtained in perpendicular directions through the jet. The symmetry in the profiles was used to determine the location of the jet axis. The radial (u) and axial (v) velocity components (with respect to the jet axis) were measured in somewhat coarse increments over the entire confined flow-field region to map the recirculation patterns which are a characteristic of the confined nature of the radial outflow. In addition to this mapping of the entire flow field, two sets of more finely spaced measurements were obtained for each configuration (Fig. 1). The axial velocity component was measured in a region centered on the jet axis and extending over a radius of 1.75 nozzle diameters. Obstruction of the laser beams by the nozzle and target plates prevented v-measurements from being obtained in a region very close to these plates. Hence, the v-measurement grid extended in the axial (z) direction to within 4.5 mm of the surfaces as shown in Fig. 1. The radial velocity component was obtained in a non-uniform grid with more measurement loca-

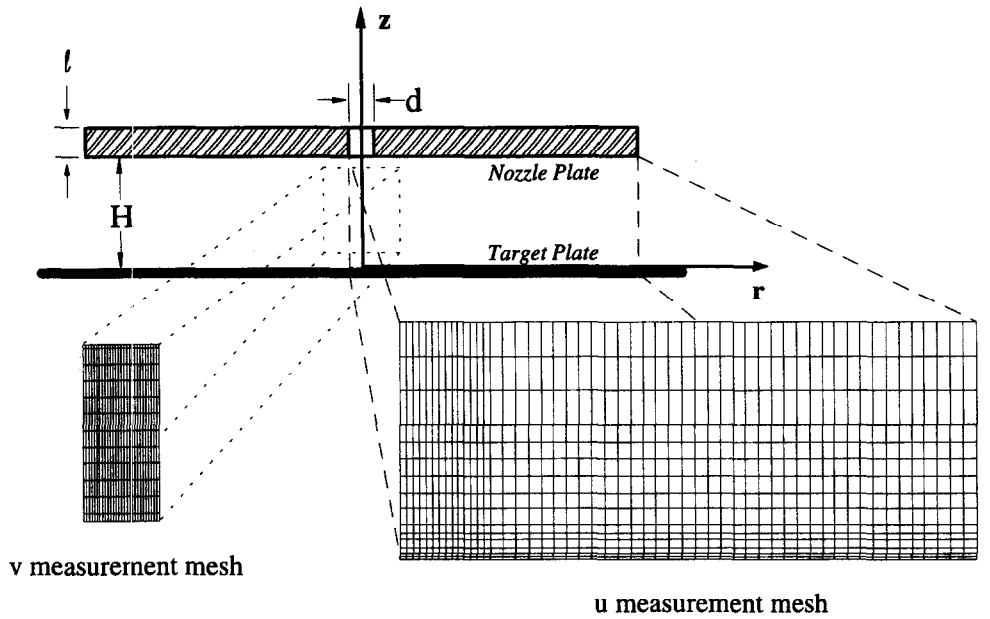

Fig. 1. Schematic diagram of the experimental impingement configuration and measurement locations for the radial (u) and the axial (v) velocity components; in addition to these fine meshes, u–v data were obtained in a coarser mesh throughout the flow field.

tions in the regions of interest: as seen in Fig. 1, the mesh was most dense close to the target plate and near stagnation.

The uncertainty in setting the average jet velocity through the rotameters was minimized by calibration and estimated to be 4% at $Re = 8500$ (for $d = 6.35$ mm) decreasing to 1% at $Re = 23{,}000$ (for $d = 3.18$ mm). The uncertainty in the velocity measurements obtained using the velocimeter was estimated to be less than 2%.

RESULTS AND DISCUSSION

Velocity and turbulence measurements are presented in this section to describe the flow field in the recirculation pattern in the confined outflow, the development of the jet after exiting the nozzle (including the potential core), and the development of the flow along the impingement surface.

Recirculation pattern in the confined outflow

A unique feature of submerged and confined jets is the presence of a toroidal recirculation zone in the outflow region. Figure 2 illustrates the recirculation pattern which is a characteristic of the effect of the confining top plate on the flow field. The results are shown at three different Reynolds numbers for a nozzle diameter of 6.35 mm and a nozzle-to-plate spacing (H/d) of 3. The toroid moves radially outward and closer to the target plate as the Reynolds number increases. For the 6.35 mm nozzle at $H/d = 3$, the center of the toroid moves radially outward from 7.8 d to 9.6 d and from a location 1.4 d from the target plate to 1.2 d away as Re is increased from 8500 to 23,000. The effect of nozzle-to-target plate spacing on the flow pattern is shown in Fig. 3 for a 6.35 mm nozzle at $Re = 8500$. Increasing the nozzle-to-target plate spacing also moves the center of the toroid radially outward (from 7.8 d to 9.5 d in this case), but its distance from the target plate remains unchanged.

These changes to the recirculation pattern in response to changes in both the Reynolds number and the nozzle-to-target plate spacing are consistent with flow visualizations previously obtained for this configuration [14, 15]. In jet impingement heat transfer, the presence of the confining top wall would thus cause fluid heated by the target plate to recirculate and become entrained into the impinging jet. This could be a contributing effect in the lower heat transfer coefficients obtained in confined jets relative to the unconfined case.

Pre-impingement jet

Figure 4(a) shows a typical plot of the velocity profiles (normalized with the mean exit velocity of the jet) in the potential core. The normalized velocity profiles for all three Reynolds numbers tested were similar; Fig. 4(a) is for $Re = 8500$ and $d = 6.35$ mm. Close to the nozzle exit, it is seen that the profile is neither uniform nor fully-developed. The velocity profile widens (the jet spreads) as ambient fluid is entrained into the jet. Hrycak *et al.* [5] described the linear rate of spread of free jets. Measurements in the present study of submerged and confined jets also display linearity in the widening of the jet. The dashed lines in Fig. 4(a) are placed at the position where the axial velocity decreases to 0.05 v_c. The dotted lines, placed at 0.95 v_c, show the degradation of the potential

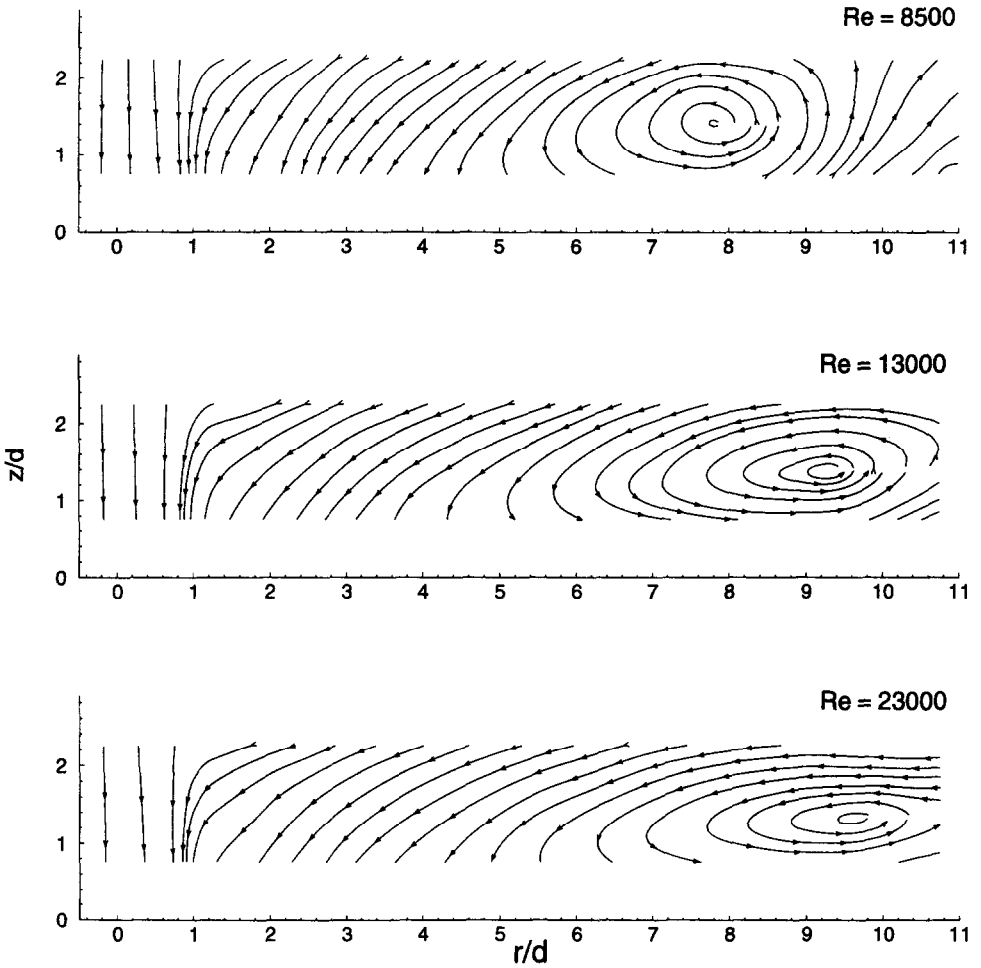

Fig. 2. Streamlines illustrating the recirculating flow patterns for $d = 6.35$ mm and $H/d = 3$ at $Re = 8500$, 13,000 and 23,000.

core due to the transfer of momentum across the jet as it widens. From the results, it may be deduced that the potential core is longer than $H/d = 4$. Since this study deals with confined jet impingement, and physical extent of confinement is fixed, the experiments were restricted to $H/d \leqslant 4$. The effect of confinement on the length of the potential core could thus not be systematically characterized.

Turbulence intensities in the potential core for the same case as considered in Fig. 4(a) ($d = 6.35$ mm, $Re = 8500$, and $H/d = 4$) are plotted in Fig. 4(b). Close to the nozzle exit, peaks in turbulence occur at the edges of the nozzle ($r/d = 0.5$). As the jet develops, the peaks decrease in magnitude as the turbulence diffuses through the jet. By the time the target plate is encountered, the turbulence levels in the figure are seen to have become nearly uniform across the jet. The results also show that the centerline turbulence levels increase with axial distance from the nozzle exit: the centerline turbulence increases for the case in Fig. 4(b) from 10.2% at a location 4.4 mm from the nozzle exit to 16.5%, 21.4 mm away from the exit. These trends in the diffusion of turbulence levels through the jet as well as the increase of turbulence levels with distance from the nozzle plate agree with observations for unconfined air jets [4]. It may be recalled that the nozzle aspect ratio of the cases studied results in a still-developing profile at the nozzle exit, and that turbulence levels measured are specific to this nozzle configuration.

Figure 5 shows the normalized axial velocity at the jet centerline (v_c/V_j) as a function of distance from the nozzle exit. The centerline velocity decreases gradually over a distance of 2.5 nozzle diameters from the jet exit. Over the next 1.5 d of distance, as the target plate is approached, the centerline velocity drops rapidly. These results appear to agree with those reported by Gardon and Akfirat [4], that a submerged impinging jet propagates as a free (non-impinging) jet to within a distance of 1.2 nozzle diameters from the impingement surface, at which state it decelerates rapidly. For unsubmerged jets, however, Stevens *et al.* [2] report that the target plate influences the pre-impingement jet only up to a distance of 0.5 d from the plate. In contrast to the velocities, centerline turbulence levels were shown to increase [17] throughout the devel-

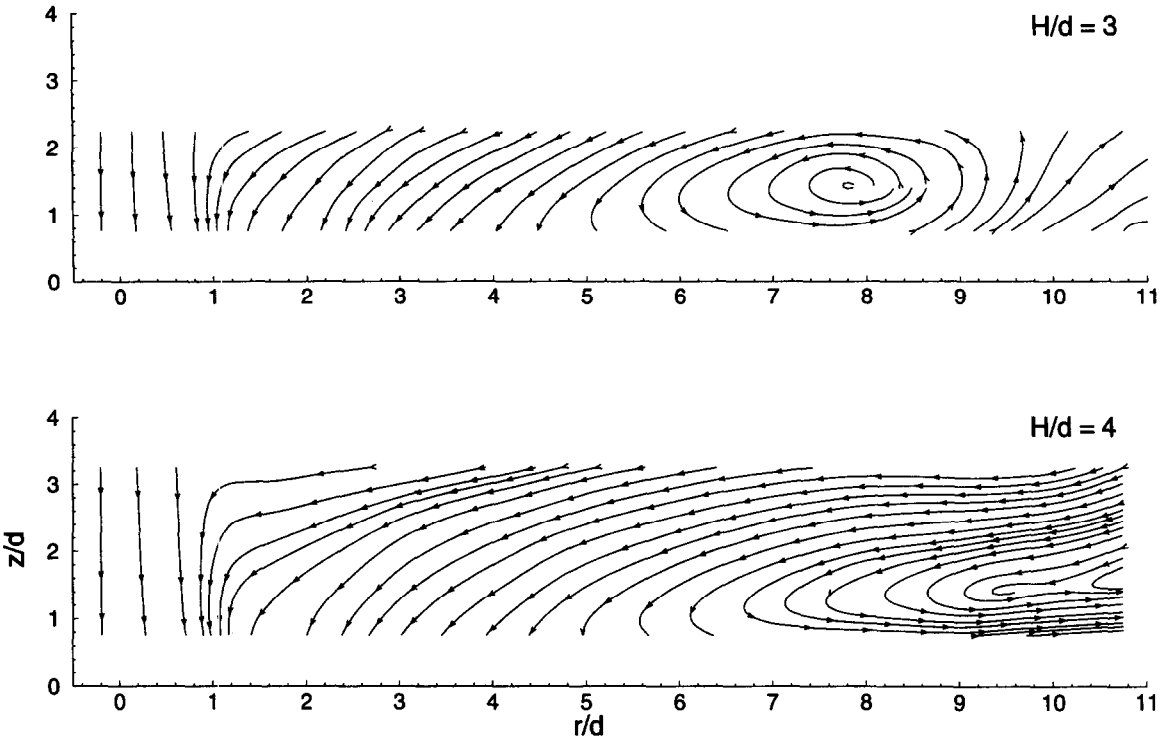

Fig. 3. Streamlines illustrating the recirculating flow patterns for $d = 6.35$ mm and $Re = 8500$ for $H/d = 3$ and $H/d = 4$.

opment of the jet as the turbulence at the walls of the nozzle as well as that generated subsequently due to shear interactions diffuse to the center of the jet. Therefore, as nozzle-to-target plate spacing is increased, the centerline velocities at the impingement surface are smaller, but turbulence levels are larger than at the nozzle exit. Heat transfer measurements [14] show slightly increasing levels of stagnation Nusselt number as H/d is increased (for $H/d \leqslant 4$), suggesting that turbulence levels are more significant to stagnation Nu than velocities.

At small nozzle-to-target plate spacings, diameter alone is seen to affect Nu in the range $r/d \leqslant 1$ [9, 13, 17]. An increase in nozzle diameter results in significantly higher stagnation Nu with all other parameters (Re, Pr, H/d) held constant. A comparison of the two nozzle diameters of this study showed higher centerline velocities and turbulence levels (both normalized with jet exit velocity) throughout the development of the larger jet, both conditions contributing to the higher Nu at the stagnation point.

Flow along the impingement surface

Radial-velocity profiles along the target plate show a maximum velocity near the plate for small r/d. Profiles are shown in Fig. 6(a) in the region close to the impingement surface for $d = 3.18$ mm and $H/d = 4$ at $Re = 23{,}000$. The development of these profiles is further discussed later, in Figs 7 and 8. When the velocities were normalized with the mean jet exit velocity, no influence of Reynolds number was detectable in the radial velocity profiles.

One descriptor of the wall-jet development is the zero-velocity plane separating the region in the flow characterized by radially outward velocities from the region with radially inward flow as shown by the dashed line in Fig. 6(b). The wall-jet development so defined was minimally affected by the size of the nozzle diameter or the Reynolds number. The slope of the zero-velocity plane characterizing the wall-jet development remained nearly constant for all cases, ranging from 0.11 to 0.15.

A comparison of the radial velocity profiles at three nozzle-to-target plate spacings is shown in Fig. 6(c); the $d = 6.35$ mm and $Re = 13{,}000$ case is shown to best illustrate the trends. The profiles show that decreasing H/d leads to an increase in the magnitude of the peak velocity. At small r/d the position of the peak is also shifted further away from the target plate for the smaller H/d. The effects of changes in H/d become negligible beyond $r/d \approx 3$.

The radial velocity is shown in Fig. 7(a) and (b) as a function of radial position at several distances (z/d) from the target plate with a Reynolds number of 23,000, $H/d = 4$ and $d = 3.18$ mm. Very near the target plate ($z/d \leqslant 0.1$) the radial velocity exhibits a maximum value at $r/d = 1$ as seen in Fig. 7(a). The magnitude of the maximum in the profile is 0.89 V_j at $z/d = 0.02$, decreasing to 0.63 V_j further from the plate at $z/d = 0.1$. With further radial travel, these differ-

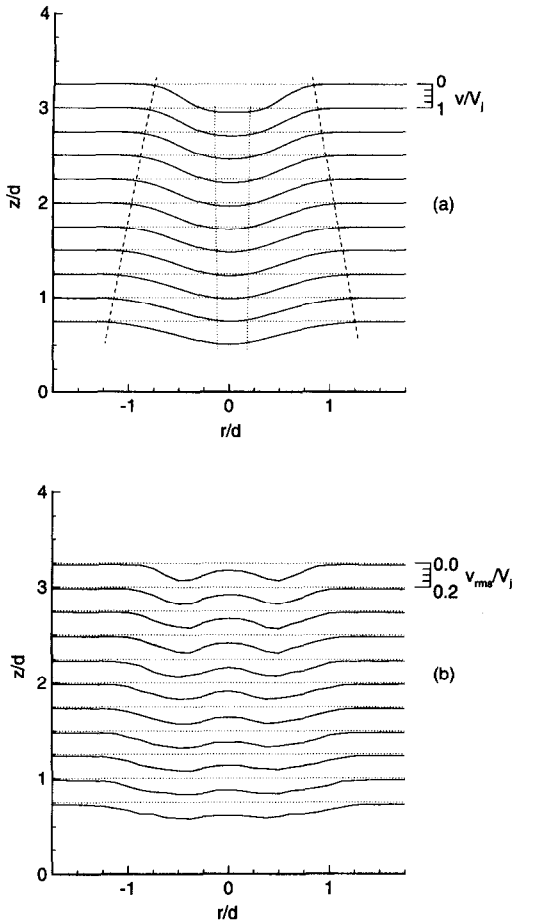

Fig. 4. Mapping of the pre-impingement jet for $d = 6.35$ mm, $H/d = 4$ and $Re = 8500$; (a) normalized velocity profiles through the jet showing jet spreading and decay of the potential core; the dashed lines indicate the extent of the jet, and the dotted lines the potential core; and (b) normalized axial turbulence intensity. (The target plate is located at $z/d = 0$, the nozzle plate at $z/d = 4$).

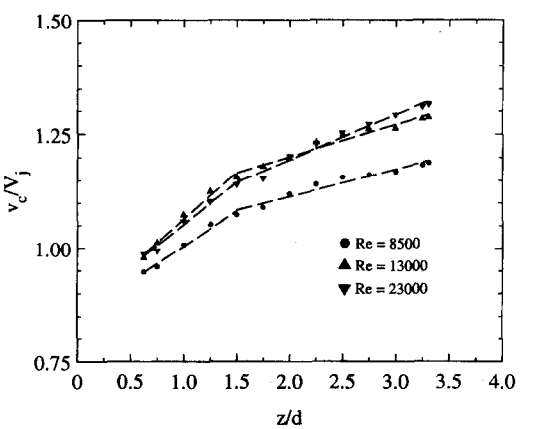

Fig. 5. Normalized centerline velocity measurements for $d = 6.35$ mm and $H/d = 4$, at $Re = 8500$, 13,000 and 23,000. (The nozzle exit is at $z/d = 4$, and the target plate at $z/d = 0$.)

ences in velocity with z/d show a reversed trend, with a complete crossover occurring at $r/d = 3$. This crossover corresponds to a change in shape of the radial velocity profiles, $u(r)$, with the peak in the profile moving away from the target plate (this is also brought out in Fig. 8(b) to follow). All the velocities then decelerate (in a narrow band) to zero at $r/d \approx 16$).

Further away from the target plate ($z/d \geqslant 0.2$), the magnitude of the maximum velocity decreases and its location shifts toward the jet centerline as seen in Fig. 7(b). Negative velocities can be seen for $r/d > 0.75$ reflecting the recirculation pattern in the fluid. At large r/d ($\geqslant 16$) the radial velocity becomes negligible at all vertical locations in the confined flow field. It is seen from Fig. 7(b) that the effect of the impingement surface on the flow is not significant for $z/d \geqslant 1.25$, since at this location the radial component of velocity is very small.

The development of the wall jet can be seen more clearly in Fig. 8(a). As the radius increases from 0 to 1 d, the magnitude of velocity increases rapidly. The position of the maximum in radial velocity occurs at the measurement location nearest the target plate ($z/d \approx 0.02$) and $r/d = 1$. Beyond r/d of 1, the velocity decreases again as seen in Fig. 8(b), due to the increase in cross-sectional area as the jet spreads radially. A slight shift in the location of peak velocity away from the target plate is also noticed as r/d increases. These findings are consistent with the free-jet results of Stevens and Webb [1], except that in the latter, the shift of the peak velocity away from the wall is quite pronounced.

The influence of nozzle-to-target plate spacing on the location and magnitude of the peak radial velocity is illustrated in Fig. 9(a). The figure shows normalized radial velocity profiles very near the target plate ($z/d = 0.04$) at $Re = 23{,}000$ and $d = 6.35$ mm for three spacings. The magnitude of the peak velocity increases as H/d is reduced, from 0.60 V_j at $H/d = 4$ to 1.17 V_j at $H/d = 2$. The location of the peak velocity does not change significantly (remaining at $0.75 < r/d < 1$ for all spacings).

Increasing the nozzle diameter reduces the magnitude of the peak velocity while moving its radial location nearer to the jet axis. The normalized radial velocity is plotted for both nozzle diameters very close to the target plate ($z/d = 0.04$) for $Re = 23{,}000$ in Fig. 9(b). Increasing the nozzle diameter from 3.18 to 6.35 mm reduces the magnitude of the peak radial velocity from 0.85 V_j to 0.60 V_j while moving the location from $r/d \approx 1$ to $r/d \approx 0.75$ in this case. All curves show a subsequent deceleration with increasing r/d.

The turbulence intensities corresponding to the radial-velocity profiles discussed in Fig. 6(a) are presented in Fig. 10(a). Even at small r/d, the profiles show significant turbulence levels. The turbulence levels increase in magnitude up to $r/d \approx 2$ (which is the location identified for the onset of transition), and gradually decrease thereafter. These trends are better

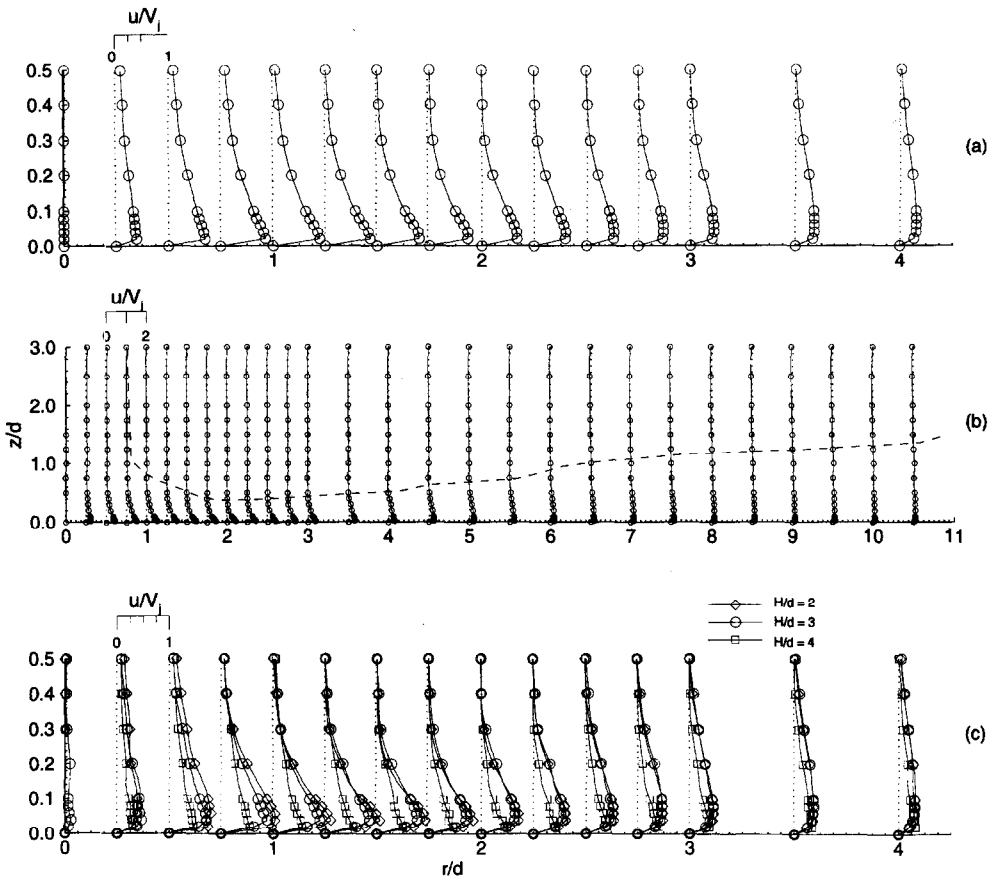

Fig. 6. Profiles of normalized local radial velocity through the stagnation and wall jet regions: (a) $d = 3.18$ mm, $H/d = 4$, and $Re = 23{,}000$; (b) the same case showing wall jet development; and (c) nozzle-to-target plate spacings of 2, 3 and 4, with $d = 6.35$ mm and $Re = 13{,}000$.

illustrated in Fig. 11. Increasing the nozzle-to-target plate spacing results in a decrease in turbulence levels near the target plate. A comparison of three nozzle-to-target plate spacings for the 6.35 mm diameter nozzle and $Re = 13{,}000$ is shown in Fig. 10(b). The effect of nozzle-to-target plate spacing decreases as r/d increases, becoming negligible beyond $r/d \approx 3.5$.

Figure 11 shows the radial distribution of the turbulence intensities measured at different distances from the target plate for a nozzle diameter of 3.18 mm with $H/d = 4$ and $Re = 23{,}000$. Measurements near the plate show a maximum level of turbulence of 17.8% at $r/d = 2$ (for $z/d \sim 0.1$), signifying the transition from a laminar to a turbulent boundary layer. As z/d increases, the turbulence levels decrease and move radially outward as the turbulence diffuses through the boundary layer. At large z/d a second region of high turbulence can be seen to occur at $r/d = 0.5$ (corresponding to the edge of the nozzle itself). The turbulence in this region also diffuses through the flow radially, resulting in two local maxima in the intermediate range of z/d.

The results from this study showed that for the range of turbulent flow rates ($8500 \leqslant Re \leqslant 23{,}000$) and nozzle-to-target plate spacings ($2 \leqslant H/d \leqslant 4$) studied, the magnitude of the radial turbulence levels are not affected by a change in Reynolds number. Furthermore, the location where transition occurs was found not to change with Reynolds number. Stevens and Webb [1] reported higher peak levels of turbulence at higher Re in free-surface jets, but their data were for a narrower nozzle-to-target plate spacing of one and a fully developed jet. Higher peak levels of turbulence are observed for smaller nozzle-to-target plate spacings (21.8% at $H/d \approx 2$ compared to 18.6% at $H/d \approx 4$), as shown in Fig. 12(a). The location of transition to turbulence, identified by the r/d at which u_{rms}/V_j drops sharply, moves radially outward as H/d is increased. Similarly, secondary peaks in heat transfer are more pronounced at smaller H/d and move radially outward for increasing H/d [14]; however, the radial location of the secondary peaks in heat transfer occur further from the jet axis than the location of peak turbulence levels at the wall. The confined air jet study of Gillespie *et al.* [10] also shows that secondary peaks in heat transfer occur downstream from the point of transition, in the region where the flow has become fully turbulent. Figure 12(b) shows turbulence measurements for two nozzle diameters at $H/d = 4$ and $Re = 23{,}000$. The larger nozzle exhibits only

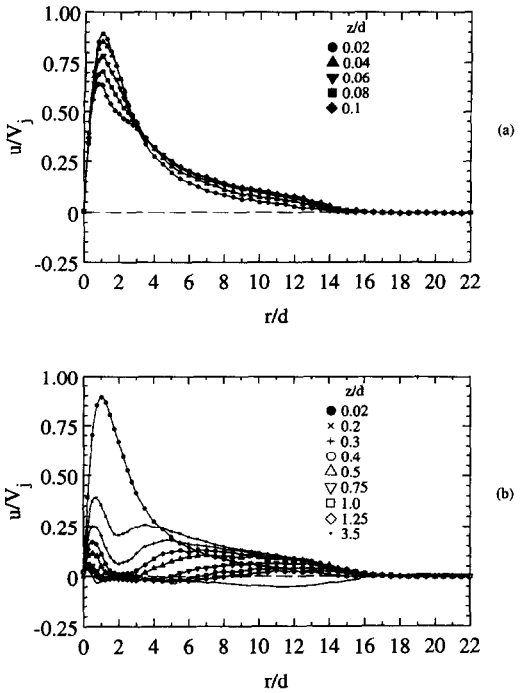

Fig. 7. Normalized radial velocities at different distances from the impingement surface for $d = 3.18$ mm, $H/d = 4$, and $Re = 23{,}000$: (a) $0.02 \leqslant z/d \leqslant 0.1$; and (b) $0.02 \leqslant z/d \leqslant 3.5$.

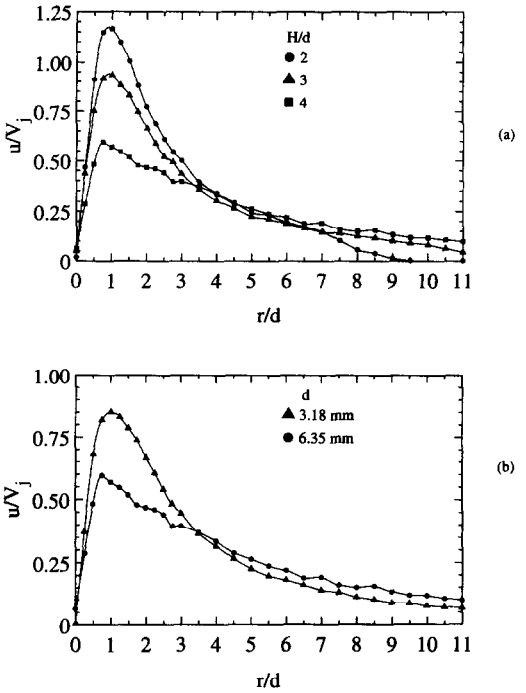

Fig. 9. Effect of (a) nozzle-to-target spacing ($d = 6.35$ mm) and (b) nozzle diameter ($H/d = 4$) on radial velocity near the target plate ($z/d = 0.04$) for $Re = 23{,}000$.

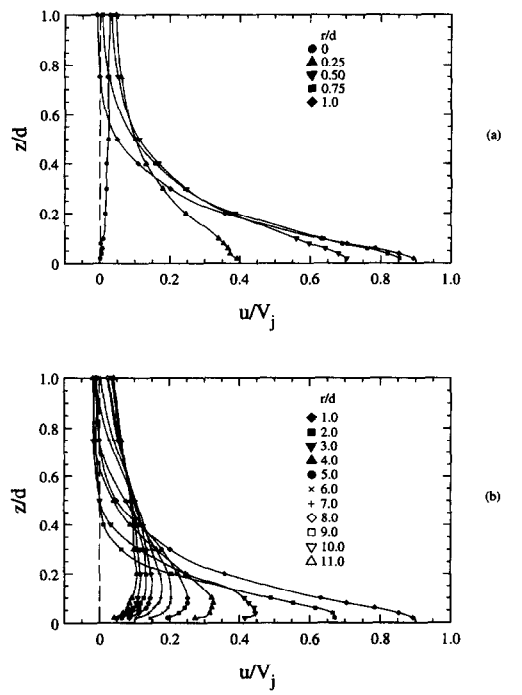

Fig. 8. Normalized radial velocities at different radial locations from the jet centerline for $d = 3.18$ mm, $H/d = 4$, and $Re = 23{,}000$: (a) $0 \leqslant r/d \leqslant 1$; and (b) $1 \leqslant r/d \leqslant 11$.

slightly higher levels of the radial component of turbulence over $r/d < 4$, as opposed to the much more significant difference in the axial component of turbulence levels seen in the pre-impingement jet measurements [17]. Correspondingly, the effect of nozzle diameter in Nusselt number distribution is significant in the stagnation region, but diminishes with distance from the jet axis [13].

CONCLUSIONS

The flow field of a confined and submerged impinging liquid jet was investigated through velocity and turbulence measurements using laser-Doppler velocimetry. A toroidal recirculation zone observed in previous flow visualization studies was mapped. The location of the center of the toroid moved radially outward, both with an increase in Reynolds number and with an increase in nozzle-to-target plate spacing. The center of the toroid moved nearer to the target plate with an increase in Reynolds number. The maximum velocity in the wall jet region occurred very close to the impingement plate for $r/d \approx 1$, with the maximum turbulence levels occurring at $r/d \approx 2$. An increase in the nozzle-to-target plate spacing was shown to reduce the magnitudes of the radial velocities as well as the peak turbulence intensities in the flow field. Increasing the nozzle diameter resulted in a decrease in peak radial velocity, but an increase in peak turbulence levels. These differences became neg-

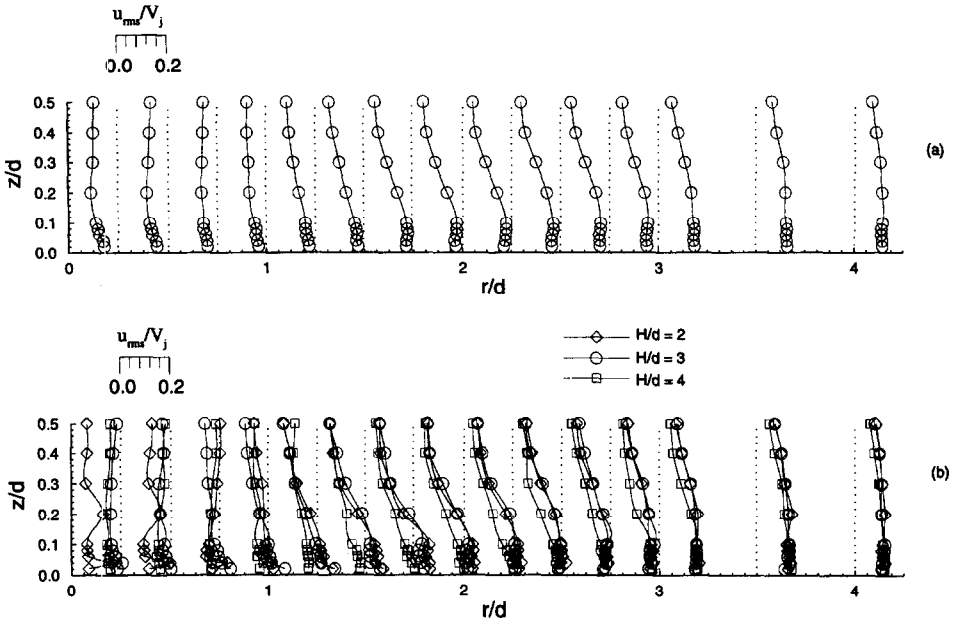

Fig. 10. Turbulence profiles (normalized with jet exit velocity) through the stagnation and wall jet regions for (a) $d = 3.18$ mm, $H/d = 4$, and $Re = 23{,}000$; and (b) $H/d = 2$, 3 and 4, $d = 6.35$ mm, and $Re = 13{,}000$.

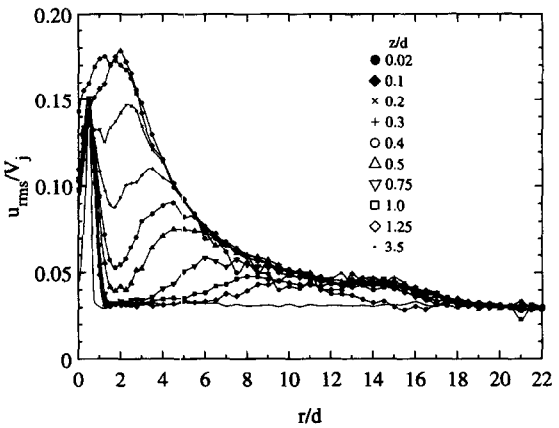

Fig. 11. Turbulence intensities at different distances (z/d) from the impingement surface for $d = 3.18$ mm, $H/d = 4$, and $Re = 23{,}000$.

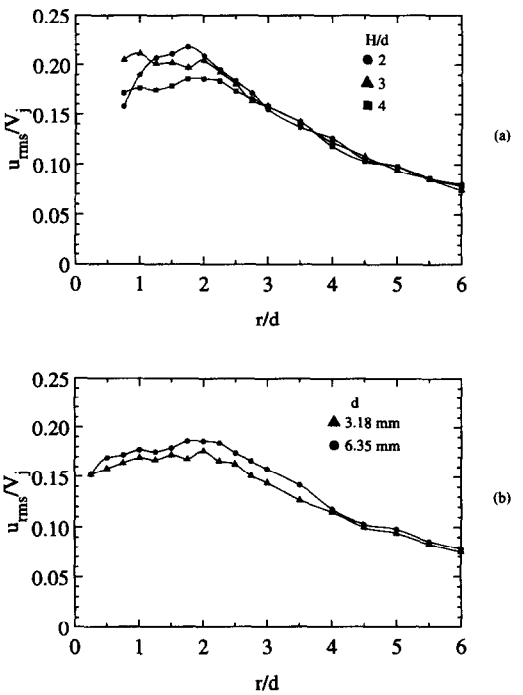

Fig. 12. Effect of (a) nozzle-to-target spacing for $d = 6.35$ mm and (b) nozzle diameter for $H/d = 4$ on turbulence intensities near the target plate ($z/d = 0.04$) at $Re = 23{,}000$.

ligible for $r/d \geq 4$. Comparisons were made with flow-field results from free jets and submerged but unconfined jets in the literature.

Acknowledgements—Partial funding for this work through a research grant from Cray Research Inc. of Chippewa Falls, Wisconsin, is gratefully acknowledged. This material is based upon work supported under a National Science Foundation Graduate Research Fellowship to JAF.

REFERENCES

1. Stevens, J. and Webb, B. W., Measurements of the flow structure in the radial layer of impinging free-surface liquid jets. *International Journal of Heat and Mass Transfer*, 1993, **36**, 3751–3758.
2. Stevens, J., Pan, Y. and Webb, B. W., Effect of nozzle configuration on transport in the stagnation zone of axisymmetric, impinging free-surface liquid jets: Part 1—Turbulent flow structure. *Journal of Heat Transfer*, 1992, **114**, 874–879.
3. Pan, Y., Stevens, J., and Webb, B. W., Effect of nozzle configuration on transport in the stagnation zone of axisymmetric, impinging free-surface liquid jets: Part 2—Local heat transfer. *Journal of Heat Transfer*, 1992, **114**, 880–886.
4. Gardon, R. and Akfirat, J. C., The role of turbulence in determining the heat-transfer characteristics of

impinging jets. *International Journal of Heat and Mass Transfer*, 1965, **8,** 1261–1272.
5. Hrycak, P., Lee, D. T., Gauntner, J. W. and Livingood, J. N. B., Experimental flow characteristics of a single turbulent jet impinging on a flat plate. NASA TN D-5690, 1970, pp. 1–32.
6. den Ouden, C. and Hoogendoorn, C. J., Local convective heat transfer coefficient for jets impinging on a plate: Experiments using a liquid technique. *Proceedings of the Fifth International Heat Transfer Conference*, Vol. 5, 1974, pp. 293–297.
7. Hoogendoorn, C. J., The effect of turbulence on heat transfer at a stagnation point. *International Journal of Heat and Mass Transfer*, 1977, **20,** 1333–1338.
8. Lytle, D. and Webb, B. W., Air jet impingement heat transfer at low nozzle-plate spacings. *International Journal of Heat and Mass Transfer*, 1994, **37,** 1687–1697.
9. Obot, N. T., Douglas, W. J. M. and Mujumdar, A. S., Effect of semi-confinement on impingement heat transfer. *Proceedings of the Seventh International Heat Transfer Conference*, 1982, **3,** 395–400.
10. Gillespie, D. R. H., Guo, S. M., Wang, Z. and Ireland, P. T., A comparison of full surface local heat transfer coefficient and flow field studies beneath sharp-edged and radiused entry impinging jets. Paper No. 96-GT-428, *International Gas Turbine and Aeroengine Congress and Exhibition*, 1996, Birmingham, U.K.
11. Schaefer, D., Incropera, F. P. and Ramadhyani, S., Planar liquid jet impingement cooling of multiple discrete heat sources. *Journal of Electronic Packaging*, 1991, **113,** 359–366.
12. Rice, R. A. and Garimella, S. V., Heat transfer from discrete heat sources using an axisymmetric, submerged and confined liquid jet. *Proceedings of the Tenth International Heat Transfer Conference*, Vol. 3, 1994, pp. 89–94.
13. Garimella, S. V. and Nenaydykh, B., Nozzle-geometry effects in liquid jet impingement heat transfer. *International Journal of Heat and Mass Transfer*, 1996, **39,** 2915–2923.
14. Garimella, S. V. and Rice, R. A., Confined and submerged liquid jet impingement heat transfer. *Journal of Heat Transfer*, 1995, **117,** 871–877.
15. Morris, G. K., Prediction of heat transfer and flow fields in submerged and axisymmetric impinging jets. M.S. thesis, Department of Mechanical Engineering, University of Wisconsin – Milwaukee, 1996.
16. Ashforth-Frost, S. and Jambunathan, K., Effect of nozzle geometry and semi-confinement on the potential core of a turbulent axisymmetric free jet. *International Communications in Heat and Mass Transfer*, 1996, **23,** 152–162.
17. Fitzgerald, J. A. and Garimella, S. V., Flow field effects on heat transfer in a confined impinging jet. *Journal of Heat Transfer*, 1997, **119,** 630–632.